DOI: 10.13009/EUCASS2023-456
Aerospace Europe Conference 2023 – 10TH EUCASS – 9TH CEAS

Wind Tunnel Investigation of an eVTOL Tiltrotor Test Bench

Catharina Moreira[⋆†]*, Nikolai Herzog*[⋆⋆] *and Christian Breitsamter*[⋆]
[⋆]*Chair of Aerodynamics and Fluid Mechanics, Technical University of Munich*
Boltzmannstr. 15, 85748, Garching bei München
catharina.moreira@tum.de
[⋆⋆]*Rolls-Royce Deutschland Ltd. & Co KG*
[†]Corresponding author

Abstract

Recent developments of electric aircraft system for eVTOL aircraft demand a better understanding of unconventional propulsion integration for both vertical lift and forward flight. A new modular wind tunnel model on a reconfigurable test stand for eVTOL aircraft is presented in this paper. The model was developed at the Chair of Aerodynamics and Fluid Mechanics of the Technical University of Munich (TUM-AER) and includes capabilities for both time-averaged and time-resolved measurements of load and pressure data. This paper describes the model design and features and presents a selection of results of its first wind tunnel tests.

1. Introduction

As the demand for efficient transportation in metropolitan areas rises, several innovative aircraft concepts have been proposed to meet this demand while also operating with low environmental and noise footprints. Particularly, electric vertical take-off and landing (eVTOL) vehicles have been the focus of research efforts for their capability to fit into the specific requirements for Urban Air Mobility (UAM) by combining the efficiency of fixed-wing aircraft with the maneuverability of rotary-wing vehicles.

However, several technical challenges to the entry into service of eVTOL aircraft still exist. Among them, it is possible to highlight the aerodynamics of propellers under non-axial inflow conditions and interactions between airframe and propulsion systems.[12] Previous investigations have explored aerodynamic characteristics of isolated propellers operating at incidence[5,6,14] and interacting propellers.[11,13] However, these test benches focused on isolated propellers, multirotor configurations or wingtip mounted propellers, and therefore provide limited insight into aerodynamic characteristics of tilting propulsion systems operating in close proximity to fixed lifting surfaces.

In order to address this issue, a new test stand for wind tunnel investigations has been developed at the Chair of Aerodynamics and Fluid Mechanics of the Technical University of Munich (TUM-AER). The test stand is a modular subscale model of a wing and propeller systems designed specifically with the purpose of obtaining both time averaged and time resolved data relevant to eVTOL aircraft, particularly considering tilting rotor concepts. The model aims to provide comprehensive experimental load and pressure data, including both static and dynamic measurements, in order to contribute to the understanding of the highly interactional aerodynamics of such systems and to provide validation data that could be used to increase confidence in computational fluid dynamic (CFD) simulations of eVTOL architectures and improve prediction tools.

This development is pursued within the context of the LuFo VI-2 project ETHAN (Safe and Reliable Electrical and Thermal Networks for Hybrid-Electric Propulsion Systems). The project is a cooperation between seven partners, including the Technical University of Munich and Rolls-Royce Deutschland, and it aims to holistically approach the development of (hybrid-)electric propulsion systems to optimize weight and efficiency without compromising overall safety of the vehicle. The traditional approach of designing redundant systems to meet high safety requirements can be complemented with high system integration and robust fault detection and isolation mechanisms to ensure a systematic and proactive approach to safety while considering weight factors. By adopting a multidisciplinary perspective that integrates various factors, such as material selection, cooling methods, power systems architecture, monitoring components and systems integration, ETHAN aims to establish a comprehensive framework to address the competing goals

DOI: 10.13009/EUCASS2023-456

effectively.

These general challenges involved with the design of (hybrid-)electric aircraft propulsion systems also affect eVTOL development efforts, which need to ensure efficiency and safety. Particularly in the case of eVTOL designs, there is also the added challenge of a wide range of potential architectures, which reflects the novelty involved in this research area, as well as uncertainty about targeted mission profiles and how vehicle performance is affected by the new technologies being employed.[9] Novel configurations with an increase in aerodynamic complexity and interaction between components that can be tilted in flight might not be well represented by conventional models traditionally used in aircraft design. Therefore, a comprehensive understanding of the aerodynamic behavior of eVTOL vehicles is of paramount importance and experimental data not only facilitate the validation of existing aerodynamic models but also serve as invaluable inputs for developing more accurate and reliable predictive tools. In fact, interactional aerodynamics are highlighted as an important factor across various domains within eVTOL development, such as noise prediction,[10] trajectory optimization[7] and aeroelastic stability.[8]

2. Experimental Setup

The following section describes the mechanical design of the wind tunnel model and the equipment employed to operate the model and to measure forces, moments and pressure data.

2.1 Mechanical Design

A new half-wing model of a hypothetical eVTOL aircraft was conceptualized, designed and built at TUM-AER in the context of the ETHAN research project. The model was designed in modular fashion to allow for investigations with the wing only (clean wing) or a wing-pylon combination, with two possible pylon mounting locations available. The conceptual design of the model includes a tilting leading edge propeller and a fixed lifter trailing edge propeller. Concept sketches are shown in figure 1. The idea behind a reconfigurable model that allows for both tilting and fixed lifter propellers at leading and trailing edge positions is to be able to represent a range of typical eVTOL architectures, including vectored propulsion concepts, lift+cruise concepts and combination concepts that integrate both vectored and fixed propulsion units. Examples of such architectures currently in development are vehicles by Joby Aviation, Archer and Vertical Aerospace.[1–3] The three dimensional concept image (right) of the eVTOL test stand shows a pylon placed at the outer position, which was also chosen for the present investigation. Additionally the model has attachment points for a pylon mounting closer to the wing root as well. These attachment points can be observed in the bottom view of figure 2, where the covers for the eight pylon mounting holes are visible.

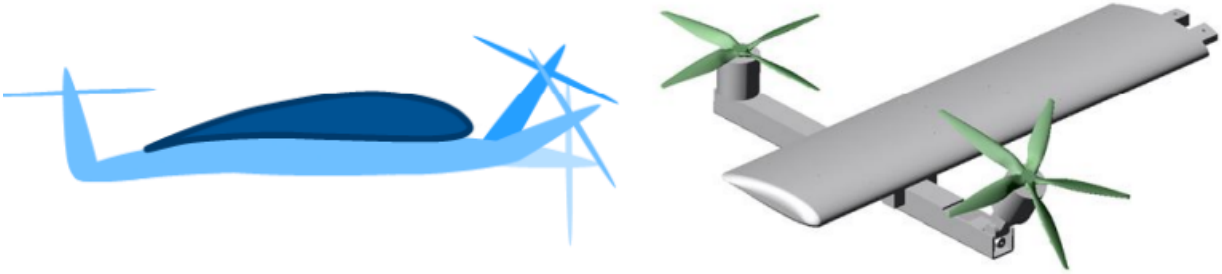

Figure 1: 2D cross-sectional view (left) and 3D CAD model of the eVTOL wind tunnel model (right).

For this investigation, the wing and a pylon with one tilting leading edge propeller were built. The wing is rectangular having a semispan of 1.1 m. The underlying airfoil is a NACA4418. It is built in aluminum alloy 7075 and the profile is hollow to allow for measurement equipment to be placed inside the wing and hidden by three removable covers located on the lower surface of the wing. Four other smaller detachable parts cover the pylon mounting holes if they are not in use. Pressure taps with a diameter of 0.3 mm on the outer surface of the wing are placed in nine different cross-sections throughout the semispan. Figure 2 shows the CAD model and the physical model without the covers, allowing the internal pressure tubes to be observed.

DOI: 10.13009/EUCASS2023-456

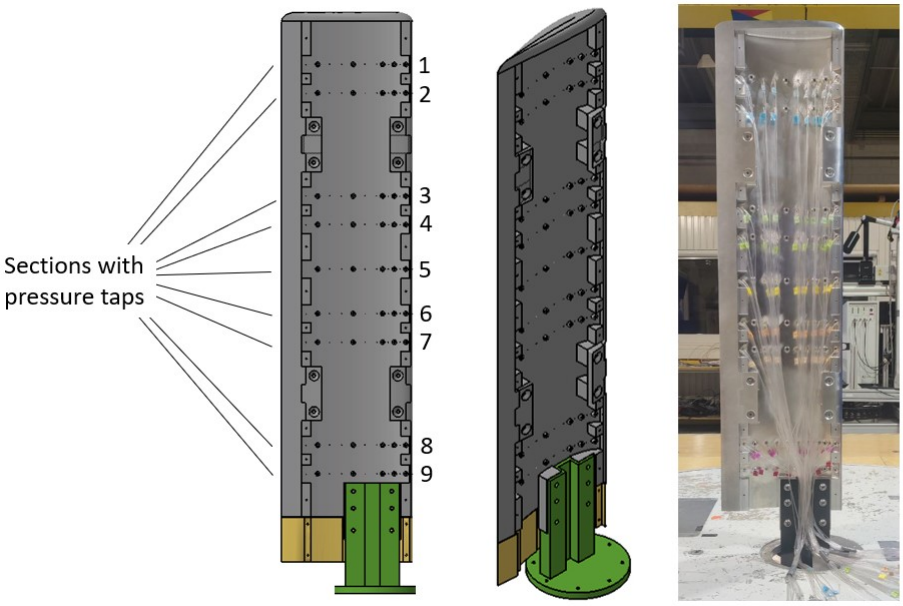

Figure 2: CAD model (left and middle) and physical wing (right) without cover pieces on the bottom surface, revealing the hollow interior. On the right, pressure tubes are visible. Also shown are the peniche (lowest wing section, shown in yellow) and the steel support with circular baseplate (shown in green).

The wing model was attached to a steel support with a circular baseplate and placed on a six-component load cell located below the floor level of the wind tunnel measurement section, which provides time-resolved load data for the entire assembly. The angle of attack (AoA) can be adjusted by rotating the entire assembly, which was placed on a turntable in the wind tunnel. Lastly, the wing ends 100 mm shy of the ground and a 3D printed cover piece (peniche) with the same airfoil shape was used to not disrupt the airflow while also excluding this particular section and potential ground effects from measurements. Both the steel support and the peniche are also visible on figure 2.

A pylon can be attached to the wing and it was designed using a rectangular steel tube that supports an electric linear actuator attached to a steel lever arm. This mechanism is responsible for tilting the load cell-motor-propeller assembly between $-10°$ and $90°$, the latter corresponding to a hover configuration. Attached to the steel lever arm, in sequence, are: a small load cell, an attachment adapter, an electric motor with custom shaft, a propeller and a spinner. The pylon structural components are built in steel to ensure high stiffness, in order to minimize the interference of structural vibrations on the time-resolved propeller load measurements.

The test stand was designed for propeller diameters in the range of 16 to 20 inches (406 to 508 mm). The present investigation was carried out with a custom built 18 in (457 mm) propeller with five blades and fixed pitch of 10 in (254 mm). The propeller has a blade shape of the commercially available APC 18x10 propeller. Because this blade shape is available off-the-shelf only as a two-bladed propeller, a five bladed propeller had to be assembled and balanced in-house for this test entry. It was operated at 4000 RPM to represent a subsonic tip Mach Number of approximately 0.3. Propeller rotation was inboard-up.

2.2 Sensors, Power and Control

The nine wing sections with pressure sensors include 23 pressure taps each, six of which are designed for transient sensors and the remaining 17 for stationary measurements. Therefore, there are in total 207 pressure holes on the surface of the wing and pressure tubes are routed through the hollow interior of the wing. Stationary taps are wired with silicone cables, which are connected to a pressure measurement device placed outside of the wind tunnel.

For this investigation, 20 transient sensors were available and therefore four groups of five sensors were used, more precisely located at the four wing sections closest to the wing tip, which are directly in the wake of the propeller, and on each section, all five sensors are positioned on the upper surface of the wing. All remaining transient pressure taps for which no transient sensors were available were adapted into stationary measurement points by using a silicone

DOI: 10.13009/EUCASS2023-456

seal. This setup is illustrated in figure 3, with the four outermost sections (Sections 1-4 in figure 2) sensored exactly as shown and the remaining sections sensored exclusively with stationary sensors at the same locations. This setup is reconfigurable in case future test entries require more transient sensors or a shift in their locations. Section 5 is positioned in the middle of the wing, with the remaining sections being positioned in pairs on each side of a pylon location at 0.5 R and 0.78 R with regard to the propeller blades (reference diameter 18 in).

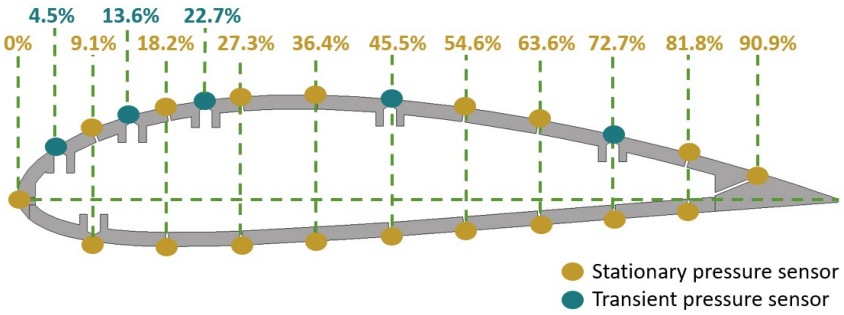

Figure 3: Schematic representation of pressure sensors on each of the wing cross-sections, with indicated values representing sensor position in percentage of the airfoil chord.

Two load cells are available for data acquisition. The locations and the coordinate systems for each load cell are illustrated in the side-by-side CAD model and physical model views shown in figure 4. The first load cell, located under the test section and supporting the entire model, can measure forces up to 5 kN in X and Z axes (see figure 4) and 15 kN in Y axis, as well as moments up to 250 Nm. Its accuracy class is 0.2% relative to full scale. The second, located directly behind the electric motor driving the propeller, can measure forces up to 500 N (Y and Z axes) /2000 N (X axis) and moments up to 20 Nm (Y and Z axes)/40 Nm (X axis) and its accuracy class is 0.5% relative to full scale. The X axis of the underfloor load cell is oriented along the wing chord, from leading to trailing edge. Also shown on the figure are the two angular parameters: the propeller tilt angle with regard to the wing (adjusted by the linear actuator) and the wing AoA (adjusted by the turntable).

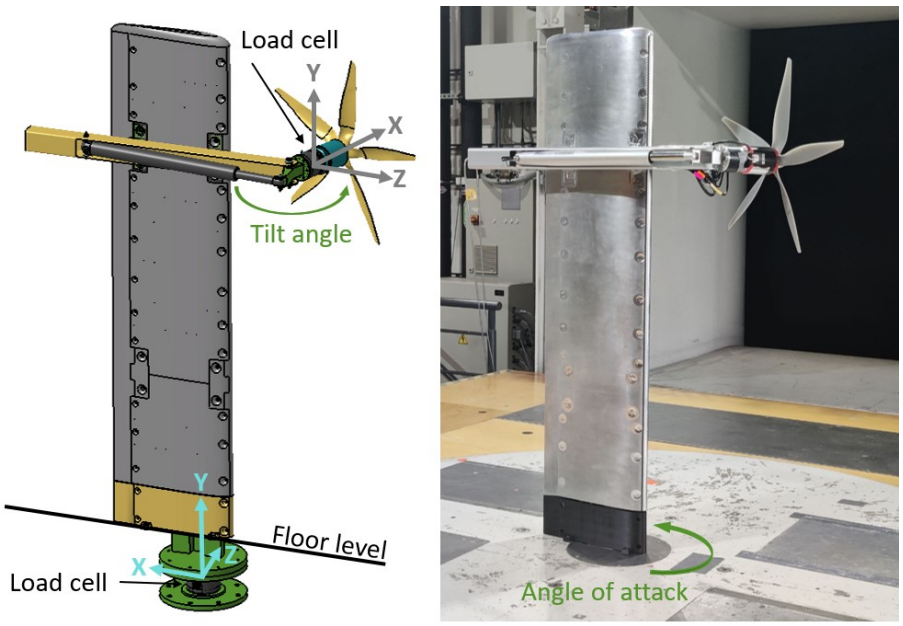

Figure 4: Bottom view of the eVTOL digital (left) and physical (right) model, indicating the position of the two load cells and the two adjustable angles, as well as the coordinate systems for both load cells.

Additionally, an optical sensor placed directly next to the motor was used to measure motor revolutions and a temperature sensor placed at the load cell behind the motor was used to monitor temperature changes due to motor heat

DOI: 10.13009/EUCASS2023-456

during the test entry. The motor selected is a brushless outrunner with maximum power of 4 kW, measuring 63 mm in diameter and 84 mm in length. It is supplied by 48 V DC converted from the grid and controlled with an electronic speed controller commanded from the wind tunnel control room.

Lastly, the linear actuator controlling propeller Tilt Angle (TA) is supplied with 24 V DC converted from the grid and controlled by an Arduino Nano board with feedback from Hall sensors integrated into the actuator itself. All cables were routed through the interior of the wing to keep the wing surfaces free. The pylon assembly can be observed in figure 5.

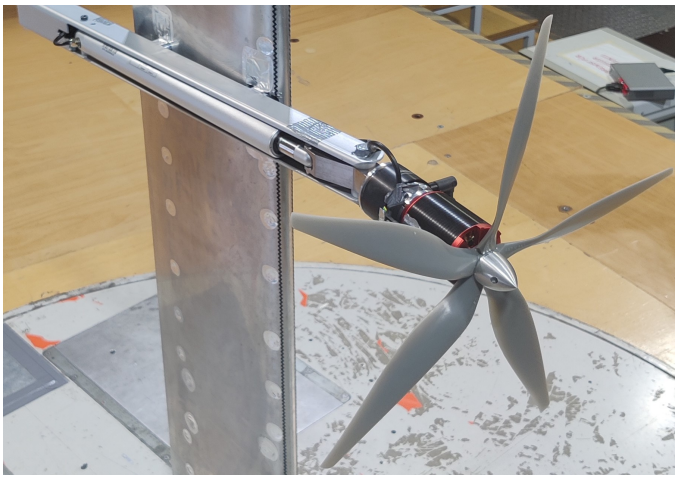

Figure 5: Detail view of pylon assembly showing support structure, linear actuator, six-component load cell, motor and 5 bladed 18x10 propeller.

In summary, the eVTOL model is a reconfigurable test stand that allows the operator to adjust wing AoA, propeller TA and propeller rotational speed from the wind tunnel control room and provides both stationary and transient pressure data over nine wing sections, as well as transient load data in three axes for both the propeller itself and the entire model.

3. Testing Conditions and Methodology

Considering this wind tunnel campaign was the first test of the new eVTOL model, one of the main goals of this investigation was to set up all required systems and ensure their functionality. In addition, the primary scientific goal of this test entry was to generate pressure distribution and load data for various tiltrotor configurations and operating points that could be encountered by an eVTOL vehicle during take-off, transition and landing phases.

The eVTOL test stand was placed in wind tunnel A of TUM-AER, which has a cross section of 1.8 m by 2.4 m, test section length of 4.8 m and maximum wind speed of 65 m/s with an open test section, as it was operated for this investigation. The turbulence level is below 0.4%, the angle divergence is below 0.2° and the uncertainty in spatial and temporal mean velocity distribution is less than 0.7%.

First, the clean wing configuration (wing only) was tested. The goals were to compare different methods for tripping the boundary layer and to establish a baseline for comparing the wing-pylon assembly results. The wing only configuration was therefore tested in three variants: no tripping (free transition), trip dots (thickness 150 μm) and a 3D printed zigzag tape (thickness 400 μm), both located at 1 cm behind the leading edge on upper and lower surfaces. Measurements for the wing only configuration were taken in groups of AoA (polars). Table 1 provides details of selected measurement conditions.

Table 1: Overview of test conditions for the clean wing configuration.

Wing AoA [deg]	**Wind speed [m/s]**
-10 to 20 (steps of 2.5)	10, 17, 25, 30

DOI: 10.13009/EUCASS2023-456

Next, the pylon was mounted for propeller-wing configuration testing. Data from both load cells and the RPM and temperature sensors were acquired simultaneously at a sampling frequency $f_s = 8\ kHz$ for 12 seconds. Measurements for wing-pylon configurations were taken individually and the load cell readings were checked in real time by operators after each measurement and tared if necessary. Table 2 indicated the parameters varied and their ranges. This investigation used a one factor at a time approach and measured all possible combinations of these factors, except the ones where the propeller was not able to provide sufficient thrust. If measured thrust became negative, the measurement was aborted. This occurred for low tilt angles and high wind speeds, as expected.

Table 2: Overview of test conditions for the propeller-wing configurations.

Wing AoA [deg]	**Wind speed [m/s]**	**Propeller TA [deg]**
-5, 0, 5, 10, 13, 15, 18, 20, 23, 25	17, 30	-10, 0, 15, 30, 45, 60, 75, 90
-90	0, 5, 10	60, 75, 90
-30, -20, -10	17, 30	90, (aligned with wind)

In order to obtain the aerodynamic loads acting solely on the wing ($F_{x,diff}, F_{z,diff}$), the measured loads from the propeller load cell had to be subtracted from the wing load cell, which supports the entire model. As shown in figure 4, the relative positioning and orientation of the coordinates systems had to be taken into account. The subtraction was carried out as

$$F_{x,diff} = F_{x,t} + F_{x,p}\cos\theta + F_{z,p}\sin\theta \tag{1}$$

$$F_{z,diff} = F_{z,t} - F_{x,p}\sin\theta + F_{z,p}\cos\theta \tag{2}$$

where θ is the TA of the configuration, the index "t" represents total loads in wing load cell coordinates and "p" represents propeller loads in propeller load cell coordinates. The aerodynamic lift and drag coefficient ($C_{L,w}, C_{D,w}$) were then obtained with the AoA, resulting in

$$c_{L,w} = (-F_{x,diff}\sin\alpha + F_{z,diff}\cos\alpha)/(\frac{\rho}{2}U_\infty^2 A) \tag{3}$$

$$c_{D,w} = (F_{x,diff}\cos\alpha + F_{z,diff}\sin\alpha)/(\frac{\rho}{2}U_\infty^2 A) \tag{4}$$

where the index "w" stands for wing and represents the aerodynamic loads acting solely on the wing,α is AoA, ρ is air density, A is wing area (semispan) and U_∞ is the freestream velocity.

4. Results

The following section presents a subset of results of the wind tunnel load cell measurements on the clean wing (without pylon and propeller) and also of propeller-wing configurations including the pylon and the front propeller in operation. In the latter case, the pylon and the built APC 18x10 5 bladed propeller were attached to the wing and the propeller was operated at 4000 RPM at different Tilt Angles (TA), which could be set by the integrated linear actuator, allowing for quick configuration changes. The aerodynamic forces and moments acting on the wind tunnel model were measured with both the wing load cell (located below the turntable) and the propeller load cell. The goal of having two load cells in the model was to be able to not only quantify the total aerodynamic forces and moments of the configuration but also to estimate the isolated effect of the propeller flow onto the wing.

The varied parameters are listed in the test matrix introduced in the previous section, including the wind tunnel velocity, the configuration AoA and the propeller Tilt Angle (TA) with regard to the wing. A subset of the results will be presented in the following to demonstrate the functionality of the new eVTOL test stand. At first the clean wing load data is presented, including comparative results between boundary layer tripping methods, followed by full configuration data and blown wing only aerodynamic data (obtained by subtraction) of various TA settings.

DOI: 10.13009/EUCASS2023-456

4.1 Clean Wing

In order to quantify the impact of different chord (c) based Reynolds numbers Re_c, the clean wing polars were measured using the wing load cell at wind tunnel speeds of $U_\infty = [10, 17, 25, 30]\ m/s$, resulting in

$$Re_c = \frac{\rho\, U_\infty\, c}{\mu} = \frac{1.12\ \mathrm{kg/m^3}\ \times\ [10, 17, 25, 30]\ \mathrm{m/s} \times 0.29\ \mathrm{m}}{1.85 \times 10^{-5}\ \mathrm{Pa \cdot s}} \tag{5}$$

$$Re_c = [1.76,\ 2.98,\ 4.39,\ 5.27] \times 10^5 \tag{6}$$

where ρ is density and μ is dynamic viscosity of air.

4.1.1 Flow Tripping Variants

Because the eVTOL model was developed with a focus on interactional aerodynamics of the transition flight phase, which likely happens very shortly after vehicle take-off and/or before landing, it is expected that low wind speeds are often present in test matrices for the model. However, low Reynolds numbers at the wing model could result in laminar flow conditions that do not represent and cannot be reasonably compared with flow conditions on real scale aircraft. For this reason, several attempts to force a turbulent boundary by means of trip dots or zigzag tape were carried out and results are presented here. A comparison of aerodynamic coefficients for the wing with no transition enforcement, trip dots (150 μm) and a zigzag tape (400 μm) with $U_\infty = 10\ m/s$ is presented in figure 6. Pressure data for one wing section (Section 6) is shown in figure 7, with other pressure sections showing similar distributions.

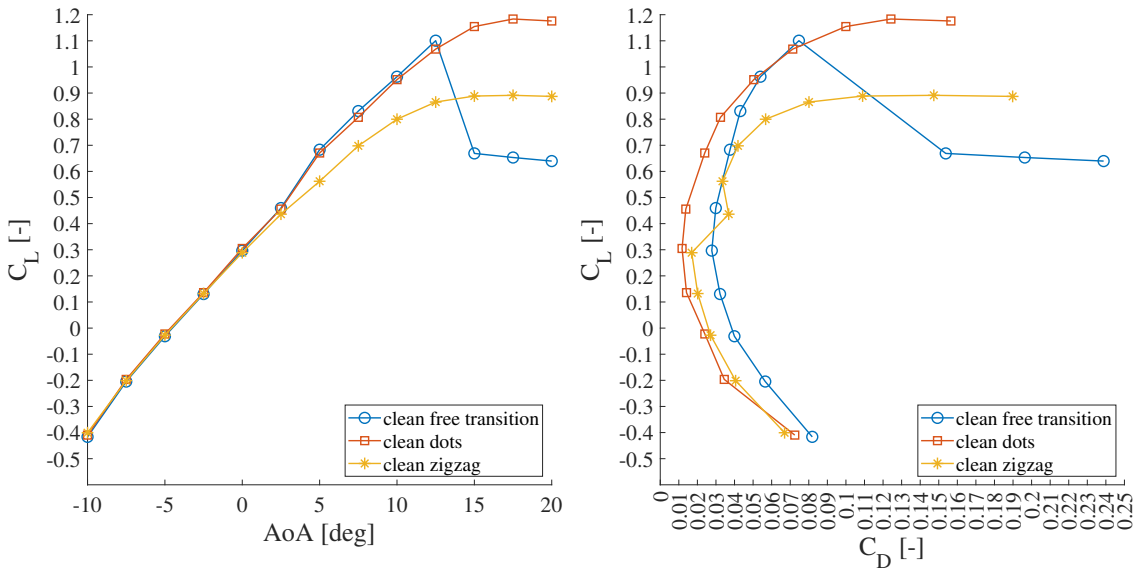

Figure 6: Aerodynamic coefficients for the clean wing (no pylon, no propeller) operating at 10 m/s with different flow transition strategies.

It can be noted that the wing operating at a low wind speed without forced transition shows an abrupt decrease in lift and increase in drag coefficients when increasing AoA beyond approximately 12 degrees. This effect could be avoided with the inclusion of small flow disturbances at the leading edge, such as the selected trip dots and zigzag tape. It is noticeable that the zigzag tape results in lower lift coefficients in the nonlinear regime, which could indicate that the selected thickness is too high for these flow conditions.

On the other hand, looking at the pressure coefficient distribution at 10 degrees AoA, a slight decrease in C_P between 30% and 55% of the chord can be observed for both the free transition case and the trip dots case, which indicates the presence of a laminar separation bubble and suggests the thickness of the dots might be too low to completely avoid laminar boundary layer effects, although they successfully improved separation behavior at higher AoAs.

DOI: 10.13009/EUCASS2023-456

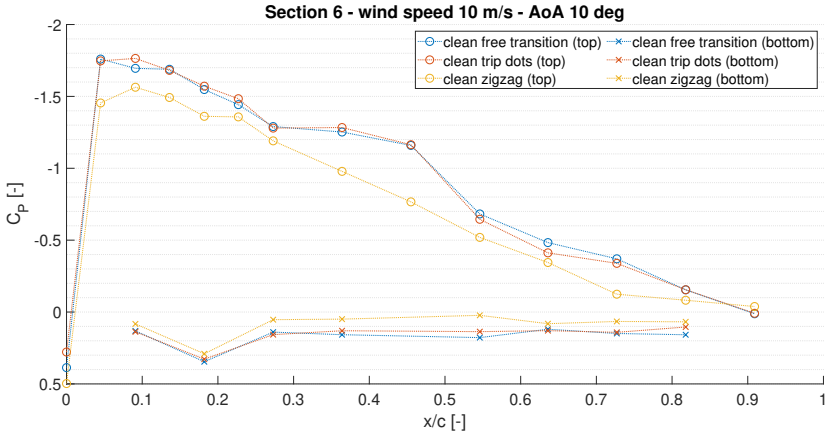

Figure 7: Pressure coefficient distribution over the chord for one airfoil section of the model with different flow transition strategies. Clean wing, wind speed 10 m/s, AoA 10 degrees.

A theoretical value for the critical thickness (k_{crit}) necessary to trip the boundary layer can be obtained with:[4]

$$k_{crit} = 26 \times x^{0.25} \times \left(\frac{\nu}{U_\infty}\right)^{0.75} = 26 \times (0.01\ \text{m})^{0.25} \times \left(\frac{1.56 \times 10^{-5}\ \text{m}^2/\text{s}}{[10, 17, 25, 30]\ \text{m/s}}\right)^{0.75} = [363, 244, 183, 159]\ \mu m \tag{7}$$

where x represents the distance from stagnation point to the disturbance, ν represents the kinematic viscosity of air and U_∞ represents freestream velocity. The theoretical values falls between the two thicknesses tested, which is in line with obtained results. Thus, the clean wing with zigzag tape was selected as base configuration for the test entry in May 2023 and the tape was present on the wing for all propeller-wing configurations tested.

4.1.2 Reynolds Number Comparison

As previously noted, the clean wing (with zigzag tape as flow tripping device) was tested at four different wind speeds to establish a baseline for comparison with propeller-wing configurations. Considering the lift coefficient C_L over AoA curves in figure 8, the linear lift regime agrees well between the different velocities. The results with velocities equal or higher than $U_\infty = 17\ m/s$ match well especially in the linear regime between $AoA = [-5, 5]°$. The curve for $U_\infty = 10\ m/s$ shows a slight derivation from all the other curves which is confirmed when looking at the drag polars in figure 8, which could possibly be associated with the disturbance introduced by the zigzag tape. The drag values within the linear regime show a decreasing trend for increasing wind tunnel speeds.

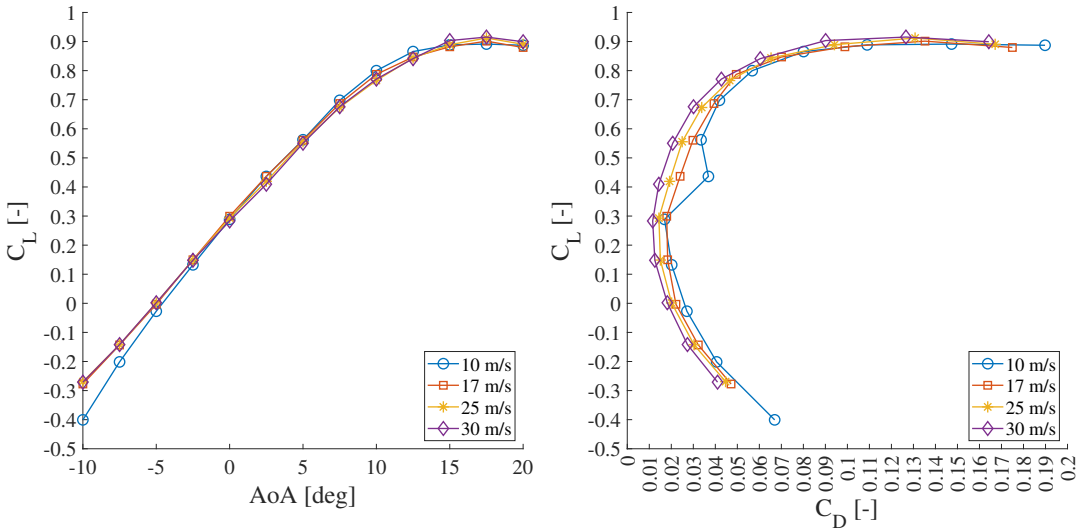

Figure 8: Lift and drag coefficients for clean wing (forced transition) at four different wind speeds.

DOI: 10.13009/EUCASS2023-456

4.2 Propeller-Wing Configurations

Next, a full configuration polar for the propeller-wing over a range of TAs from 0 to 90 degrees is analyzed. For this model, 0TA represents a configuration with the propeller axis aligned to the wing chord and 90TA represents a hover configuration. The intermediate angles are conditions through which an eVTOL aircraft hast to operate when it is transitioning between hover flight and wing-born flight. The lift and drag coefficients for the full model are compared to the results for the blown wing only, which was obtained by subtracting propeller load cell data from the wing load cell results, as explained in section 3. The wind tunnel speed for this comparison is $U_\infty = 17\ m/s$. The resulting lift and drag polars of different configurations are compared in figure 9 and the results for the wing-only loads are compared against the initial clean wing polar in figure 10. Propeller results are shown in figure 11.

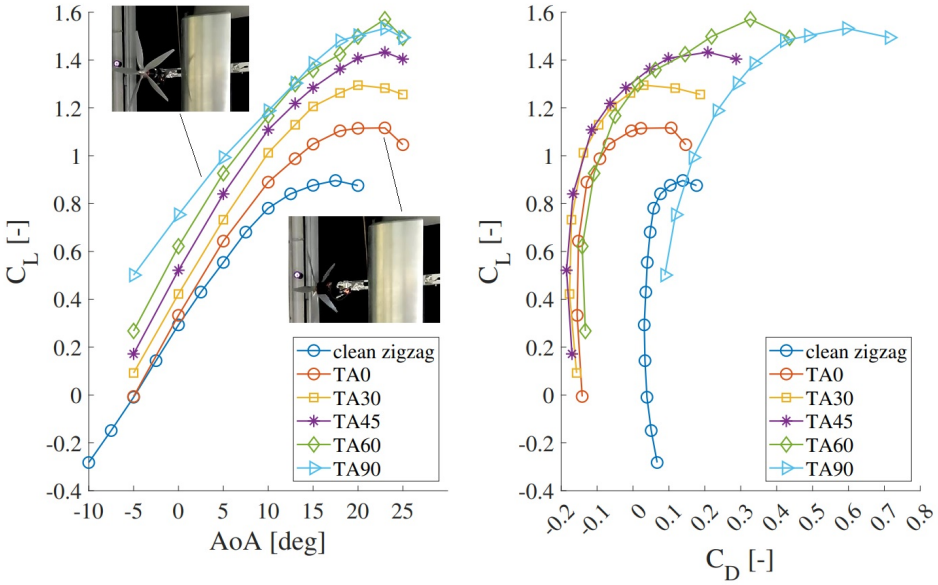

Figure 9: Lift and drag coefficients for entire model assembly with different propeller TA configurations. Wind speed 17 m/s.

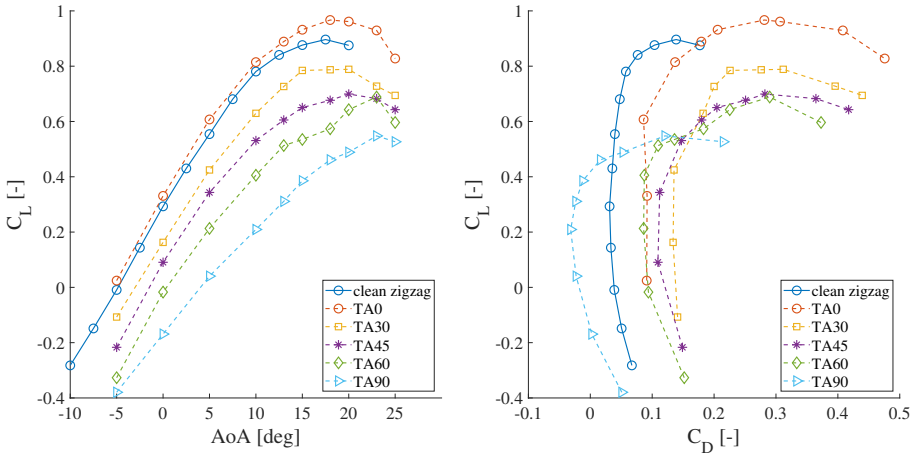

Figure 10: Lift and drag coefficients for blown wing with different propeller TA configurations, obtained by subtraction. Wind speed 17 m/s.

Noticeable on the lift polars is that the lift coefficient for the entire assembly tends to increase with tilt angle, as the direction of propeller thrust is vectored to contribute to vehicle lift. However, a comparison with blown wing lift

DOI: 10.13009/EUCASS2023-456

polars reveals that the wing contribution to lift in the propeller-wing configurations tested was lower than for a clean wing, with the exception of 0TA, which shows a slight increase in wing only lift, possibly due to increased dynamic pressure in the propeller slipstream impinging directly onto the wing.
In contrast to the clean wing, the propeller-wing assembly shows negative drag coefficients, as the total forces of the model are influenced by the thrust acting onto the configuration. However, blown wing results indicate that the wing itself is operating with higher aerodynamic drag than in a clean wing scenario., except for the TA90 configuration. The propeller coefficients are nondimensionalized with air density ρ, propeller rotational speed n and diameter D according to:

$$[C_T, C_Z] = \frac{[T, F_z]}{\rho n^2 D^4} \tag{8}$$

The coefficients show a clear trend of increasing thrust and absolute side force (Z-axis) coefficients with increased TA, with the exception of side force for TA90. Particularly with the TA90 configuration, the propeller is operated with reverse inflow as the AoA increases and the frontal cross section of the propeller assembly with regard to inflow is reduced, which could explain why the trend for propeller side force and, consequently, blown wing drag are reversed.

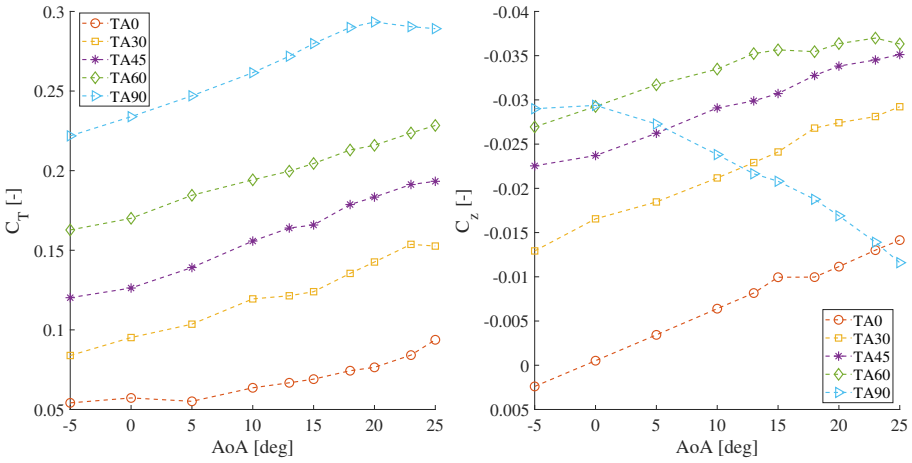

Figure 11: Thrust and side (Z-axis) force coefficients for propeller with different TA configurations while operating in the interactional flowfield of the eVTOL model (in propeller load cell coordinate system). Wind speed 17 m/s.

5. Conclusions

The development and testing of a new wind tunnel test stand suitable for innovative eVTOL aircraft has been shown. The new testing capabilities and the experiments carried out during its first wind tunnel test entry are motivated by the complex aerodynamics of tilting configurations, in particular during transition flight stages.
This wind tunnel model includes two load cells for transient load acquisition and both static and transient pressure sensors over nine wing sections. Descriptions of the mechanical design, geometry, operating conditions and supporting equipment were given and an overview of initial time-averaged results was presented.
Different boundary layer transition enforcement strategies were compared with polars and pressure data and revealed that free transition is present, while a turbulent boundary layer is enforced when applying transition devices, namely trip dots and a zigzag tape. Data for clean wing (no pylon, no propeller) configurations and propeller-wing configurations were compared, revealing a trend of increased lift and decreased drag coefficients for the entire assembly as the tilt angle of the propeller is increased (towards hover configuration). These trends are reversed when considering the forces acting solely on the wing in power on configurations. The aerodynamics involved in eVTOL transition flight are expected to be characterized by highly unsteady and separated flows producing oscillating loads onto the wing and propeller and it is clear that comprehensive experimental results including both steady and unsteady data are required to further understand these phenomena. Further experiments and analyses towards this goal, in particular of transient wind tunnel data, are planned at TUM-AER and will be enabled by the newly developed eVTOL test stand.

DOI: 10.13009/EUCASS2023-456

6. Acknowledgments

This work was funded by the German Federal Ministry for Economic Affairs and Climate Action *(Bundesministerium fuer Wirtschaft und Klimaschutz)* within the LuFo VI-2 project ETHAN (Safe and Reliable Electrical and Thermal Networks for Hybrid-Electric Propulsion Systems, FKZ: 20L2103B).

References

[1] Archer aviation. https://www.archer.com/. Accessed: 2023-06-25.

[2] Joby aviation. https://www.jobyaviation.com/. Accessed: 2023-06-25.

[3] Vertical aerospace. https://vertical-aerospace.com/. Accessed: 2023-06-25.

[4] C. Breitsamter. Strömungsphysik und Modellgesetze. Lecture Notes. Technische Universitaet München, 2012.

[5] M. Cerny and C. Breitsamter. Investigation of small-scale propellers under non-axial inflow conditions. *Aerospace Science and Technology*, 106:106048, 2020.

[6] M. Cerny, N. Herzog, J. Faust, M. Stuhlpfarrer, and C. Breitsamter. Systematic Investigation of a Fixed-Pitch Small-Scale Propeller under Non-Axial Inflow Conditions. Deutsche Gesellschaft fuer Luft- und Raumfahrt - Lilienthal-Oberth e.V., 2018.

[7] S. S. Chauhan and J. R. R. A. Martins. Tilt-wing evtol takeoff trajectory optimization. *Journal of Aircraft*, 57(1):93–112, 2020.

[8] A. Cocco, S. Mazzetti, P. Masarati, S. Van't Hoff, and B. Timmerman. Numerical whirl-flutter analysis of a tiltrotor semi-span wind tunnel model. *CEAS Aeronautical Journal*, 13:923–938, 2022.

[9] L. A. Garrow, B. J. German, and C. E. Leonard. Urban air mobility: A comprehensive review and comparative analysis with autonomous and electric ground transportation for informing future research. *Transportation Research Part C: Emerging Technologies*, 132:103377, 2021.

[10] B. Mukherjee. A preliminary investigation of propeller-wing interaction noise for evtol aircraft. Master's thesis, Pennsylvania State University, December 2020.

[11] C. R. Russell and S. Conley. The multirotor test bed - a new nasa test capability for advanced vtol rotorcraft configurations. 2020.

[12] B. M. Simmons and P. C. Murphy. Wind tunnel-based aerodynamic model identification for a tilt-wing, distributed electric propulsion aircraft. AIAA SciTech Forum 2021-1298, American Institute of Aeronautics and Astronautics, January 2021.

[13] T.C.A Stokkermans. *Aerodynamics of Propellers in Interaction Dominated Flowfields: An Application to Novel Aerospace Vehicles*. Ph.D. Dissertation, 2020. OCLC: 8692979511.

[14] M. Stratton and D. Landman. Wind tunnel test and empirical modeling of tilt-rotor performance for evtol applications. AIAA SciTech Forum 2021-0834, American Institute of Aeronautics and Astronautics, January 2021.